Journal of Computational Electronics (2022) 21:1048–1059
https://doi.org/10.1007/s10825-022-01893-x

Polymer thin film transistor vapor sensor analysis, drift suppression, and response optimization via circuit level strategy

T. Mukhopadhyaya[1] · N. McKeever[1] · H. E. Katz[1] · W. Wondmagegn[2]

Received: 15 September 2021 / Accepted: 20 April 2022 / Published online: 4 June 2022

Abstract
Organic field effect transistors (OFETs) and circuits are simulated and tested for gas analyte and humidity sensitivity. The transistors and circuits are based on two dipyrrolopyrolidone–thiophene copolymer organic semiconductor thin films. The conventional OFET structure that includes a bottom (substrate) gate and top source and drain contacts is simulated using the two-dimensional finite element method. Charge traps due to structural defects and grain boundaries are assumed to be approximately uniformly distributed in the semiconductor. The doping dependent hopping mobility model is used to model organic semiconductor vapor sensitivity of the organic active material. The effect of humidity is modeled by traps in the semiconductor. The two transistors in the series configuration are also studied for nitrogen dioxide (NO_2) and humidity sensitivity. The circuit configuration has an advantage of maintaining a significant level of analyte sensitivity under humidity exposure. This is confirmed by both simulation and experiment. At 15% humidity level, the circuit maintained 22% sensitivity to 20 ppm NO_2 exposure. Significant further improvement in analyte sensitivity and suppression of humidity effect are also predicted by simulation when the circuit is constructed from symmetric output transistors. To the best of our knowledge, this is the first study of the technique of symmetrical circuit design methodology to suppress the effect of humidity on OFET circuits while maintaining their response to gas analyte.

Keywords Doping dependent mobility · Density of states · Device simulation · NO_2 sensing · Organic field effect transistor · OFET gas sensor

1 Introduction

In addition to their typical application in flexible displays, electronic paper, radio frequency identification (RFID) tags, and smart cards [1–3], a recent research trend in organic field-effect transistors (OFETs) is testing them for novel sensing technologies for potential applications in environmental, biological, and industrial areas [4–11]. The inherent responsiveness of organic semiconductors to the surroundings makes them suitable for detection of external chemical and physical stimuli. However, this same property is also one of the detrimental factors in fabricating OFET sensors for practical sensing applications. OFETS have stability, hysteresis, and threshold voltage shift issues because of their susceptibility to environmental factors via chemical interactions, photoexcitation, and dimensional deformation [12–15]. Owing to tremendous efforts in terms of design and synthesis of novel organic semiconductors, implementation of new transistor fabrication techniques, and material interface engineering, gas analyte sensors of high sensitivity are demonstrated by various groups [16–19], including our group [9–11]. However, the reported devices have reproducibility and stability issues even when exposed to ambient atmosphere and temperature. Therefore, in addition to such described research techniques, low level circuit design is an avenue to be considered to advance the technology for practical use. For example, two different polymers that have similar drifts in air and humidity but divergent responses to gas analyte could be configured in a way to minimize humidity effects.

In addition, the charge transport in disordered organic conducting materials is based on the charge carrier hopping within energetically and spatially disordered localized

✉ W. Wondmagegn
wondmagw@tcnj.edu

[1] Department of Materials Science and Engineering, Johns Hopkins University, Baltimore, MD 21218, USA

[2] Electrical and Computer Engineering Department, The College of New Jersey, Ewing, NJ 08628, USA

states. These localized states are formed by potential wells of defects and traps [20, 21]. The energy difference between the deep trap states and the effective transport level controls the hopping rate of charge carriers. The type and density of traps in a semiconductor is the basis for the applicability of either the multiple trap and release (MTR) transport model or the variable-range hopping (VRH) model [22–25]. The variable range hopping within the Gaussian distribution density of states may result in effective percolation of charge transport paths or the relevant frontier orbitals [26]. The MTR model also assigns a controlling role to traps with energies at levels between the highest occupied and lowest unoccupied molecular orbitals [20, 27–32]. Published reports show that both MTR and VRH models have been used to analyze organic field effect transistor data [33].

To understand such complex charge transport phenomena in OFETs, physical device simulation based on the fundamental semiconductor equations such as Poisson's and continuity equations is desired. In the present work, the result of a physical simulation of transistors and circuits with and without exposure to analyte vapors is presented. NO_2 is chosen as the analyte of interest because of its status as a common, toxic, and desirably monitored pollutant [34–37]. The result is compared with experimental data. A series circuit of two transistors is also tested for humidity and analyte sensitivity.

2 Device simulation

Transistors (see Fig. 1) are structured with 200 µm channel length and 11 mm channel width. The device simulations are performed based on a drift diffusion model using Silvaco's ''ATLAS'' device simulator [38]. The polymers (Fig. 1) were described in detail in Ref. [9]; the designations "P6" and "P7" are taken from that reference for consistency. The details of fabrication and experimental characterization of the devices used in the simulation are also described in Ref. [9]. Circuits that are the main subject of this work were made from the identical individual devices.

Table 1 Summary of material and model parameters

Parameter	P6	P7
Band gap	1.3 eV	1.63 eV
Affinity	3.82 eV	3.49 eV
HOMO	−5.12 eV	−5.24 eV
LUMO	−2.18 eV	−2.45 eV
Mobility	0.12 cm^2/V s	$3.13\times10^{-3} cm^2/V$ s
Threshold voltage	7.38 V	−0.99 V
Permittivity	3	3
Intrinsic doping density	7×10^{15} cm^{-3}	1.88×10^{14} cm^{-3}
σ_1, σ_2	0.05 eV, 0.34 eV	0.05 eV, 0.34 eV
E_d	0.1 eV	0.1 eV
γ, β	10^7 cm^{-1}, 0.2	10^7 cm^{-1}, 0.2
ν_0	10^{11} Hz	10^{11} Hz
Polymer thickness	130 nm	130 nm
Oxide thickness	300 nm	300 nm
Source/drain thickness	50 nm	50 nm
Gate thickness	50 nm	50 nm
Channel length	0.2 mm	0.2 mm
Channel width	11 mm	11 mm
Interface charge	1×10^{10} cm^{-2}	1×10^{10} cm^{-2}

Gold with work function of 5.1 eV is used as source/drain electrode. SiO_2 with relative permittivity of 3.7 is used as gate dielectric as is well established for organic electronic devices [39–41]. Highly n-doped silicon with high conductivity and work function of 4.15 eV is used as the gate electrode. The optical bandgaps of P6 and P7 used in the simulation are 1.3 eV and 1.63 eV, respectively. Interface charge between the semiconductor and insulator is on the order of 1×10^{10} cm^{-2} for both P6 and P7 transistors. This quantity is extracted from the best fit by matching simulation and experiment iteratively. The band gap and electron affinity of the polymers are determined from the UV–Vis absorbance of P6 and P7 films [9]. Material parameters used in the simulation are summarized in Table 1.

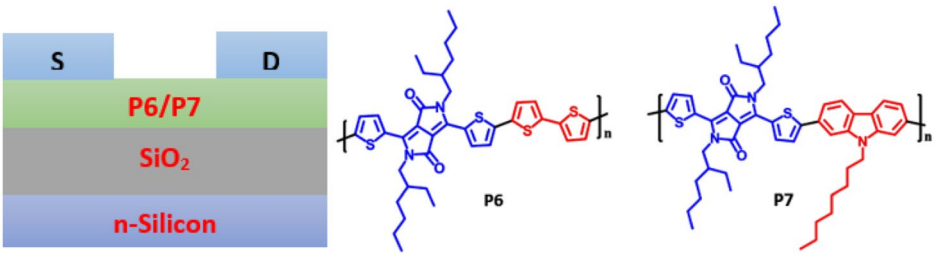

Fig. 1 P6/P7 OFET device structure used in simulations and circuits, and polymer semiconductor chemical structures

P6: poly(2,5-bis(2-ethylhex-1-yl)-2,4-dihydro-3,6-dioxopyrrolo[3,4-c]pyrrole-1,4-diyl)-alt-2,2'-5',2"-5"-2"'-quaterthien-5,5"'**-diyl)**

P7: poly(2,5-bis(2-ethylhex-1-yl)-2,4-dihydro-3,6-dioxopyrrolo[3,4-c]pyrrole-1,4-diyl)-alt-9-octylcarbazole-2,7-bis-2,2'-thiophene-5,5'-diyl)

The simulation is based on the generalized drift–diffusion equations described below [20, 42, 43],

$$\mathrm{div}(\varepsilon\nabla\psi) = q\left(n - p - N_D^+ + N_A^-\right) + Q_T \tag{1}$$

$$\frac{\partial n}{\partial t} = \frac{1}{q}\mathrm{div}\vec{J}_n + G_n - R_n \tag{2}$$

$$\frac{\partial p}{\partial t} = -\frac{1}{q}div\vec{J}_p + G_p - R_p \tag{3}$$

$$\vec{J}_n = qn\mu_n\vec{E}_n + qD_n\nabla n \tag{4}$$

$$\vec{J}_p = qn\mu_p\vec{E}_p + qD_p\nabla p \tag{5}$$

where D_n and D_p are electron and hole diffusion coefficients, respectively. G_n is electron generation rate, G_p is hole generation rate, and R_n and R_p are electron and hole recombination rates, respectively. Q_T is total fixed charge, n and p are electron and hole concentrations, respectively, q is electronic charge, N_D^+ and N_A^- are ionized donor and acceptor concentrations, ε is permittivity of the material, μ_n and μ_p are electron and hole mobilities, respectively. ψ is electrostatic potential, $\vec{J}_n$ and $\vec{J}_p$ are electron and hole current densities, respectively.

To approximate the charge localization that is a phenomenon associated with disordered semiconductors, especially organic ones, the disorder caused by the molecular structure is described by a Gaussian distribution density of states [44]. The Gaussian distribution is described by its peak density of states (N_1 and N_2), its characteristic decay energy (σ_1 and σ_2), and the reference energy level E_d, as shown in Eq. (6) [38, 45].

$$g(E) = \frac{N_1}{\sqrt{2\pi\sigma_1}}\exp\left(-\frac{E^2}{2\sigma_1^2}\right) + \frac{N_2}{\sqrt{2\pi\sigma_2}}\exp\left(-\frac{\left(E+E_d\right)^2}{2\sigma_2^2}\right) \tag{6}$$

Charge carrier mobility enhancement by trap filling phenomena [46, 47] is represented by the doping dependent mobility model (Eq. 7). Equation (8) represents the effective transport energy in a hopping system represented by the Gaussian distribution of states [13, 39, 48–50].

$$\mu_{\mathrm{tr}} = \frac{q\nu_0}{kT}\left[\int_{-\infty}^{E_{\mathrm{tr}}} g(E)\mathrm{d}E\right]^{-2/3}\exp\left[-2\left(\frac{3\beta}{4\pi}\right)^{1/3}\gamma\left[\int_{-\infty}^{E_{\mathrm{tr}}} g(E)\mathrm{d}E\right]^{-1/3}\right] \tag{7}$$

$$\int_{-\infty}^{E_{\mathrm{tr}}} g(E)\left(E_{\mathrm{tr}} - E\right)^3\mathrm{d}E = \frac{6\beta}{\pi}(\gamma kT)^3 \tag{8}$$

where μ_{tr} is the charge mobility in the effective transport hopping system, E_{tr} is effective transport level of the energy, ν_0 is the attempt-to-jump frequency, $1/\gamma$ is inverse of carrier localization radius, β is the percolation constant, q is electronic charge, k is Boltzmann's constant, and T is temperature.

3 Device and circuit simulation results

3.1 Device simulation of P6 and P7 transistors

Device simulation of transistors is performed without exposure to gas analyte or humidity. Current–voltage data generated from simulation are matched with experiment and device parameters are extracted. The simulated devices serve as the basis for the analyte and humidity sensitivity study. Figure 2 presents output and transfer current–voltage (*I–V*) characteristics of experimental and simulation results. In the figures, the black (circle) curves represent experimental data and the blue (triangle) curves represent simulation data. Figure 2a, b correspond to P6 and Fig. 2c, d correspond to P7 OFETs. Measurements and simulations of transfer characteristics shown in Fig. 2b, d are performed at − 100 V drain voltage.

Simulation data show good agreement with experimental data for both transistors. Except for the highest gate/low drain region for P6, deviations are quite minimal, and within the standard deviations of experimental data. As shown in the transfer curves, the low gate voltage plots (< − 70 V) show excellent agreement between simulation and experiment. Output curves also show good agreement except at higher gate voltage (− 40 V) where P6 transistor is showing a small deviation (statistically insignificant) in the linear region and P7 transistor is showing similar deviation in the saturation region. Trap and interface charge densities are extracted from the best fit. These parameters are listed in Table 1 and are used as initial parameters in subsequent simulations, i.e., circuit and analyte and humidity sensitivity simulations.

3.2 Circuit simulation

Circuits based on P6 and P7 transistors are simulated. Material and mobility parameters validated from device simulation, listed in Table 1, are used. The two transistors are configured in the series configuration as shown in Fig. 3. The circuit is simulated with a device and circuit level mixed mode simulation. The output voltage versus input voltage simulation result of the circuit is displayed in Fig. 4. The result serves as a basis for gas analyte sensing simulation performed in Sects. 4 and 5.

The two OFETs operated as though they were typical p-type transistors. They have common applied gate voltage but the source-drain voltage across the series circuit was the

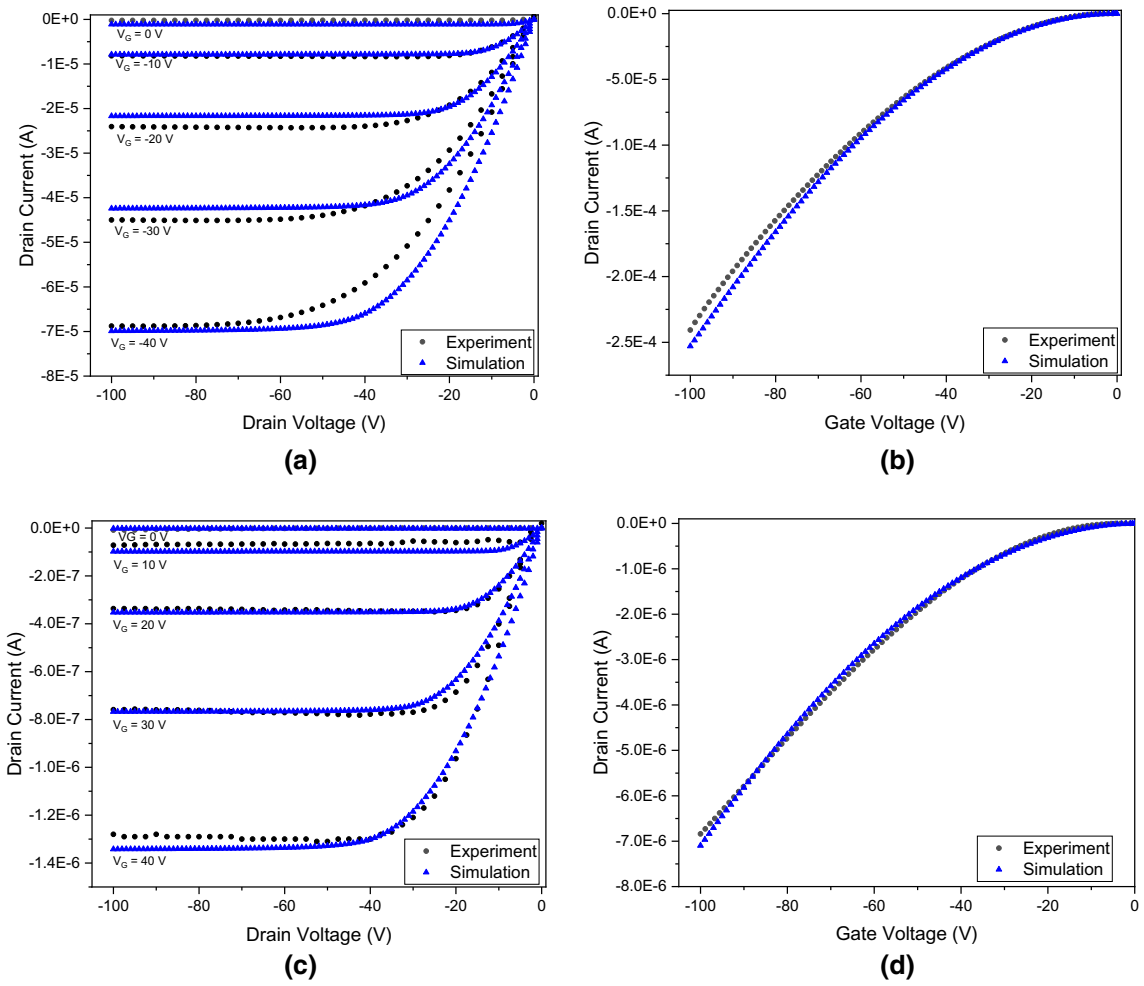

Fig. 2 **a**, **b** output and transfer curves of P6 transistor, **c**, **d** output and transfer curves of P7 transistor

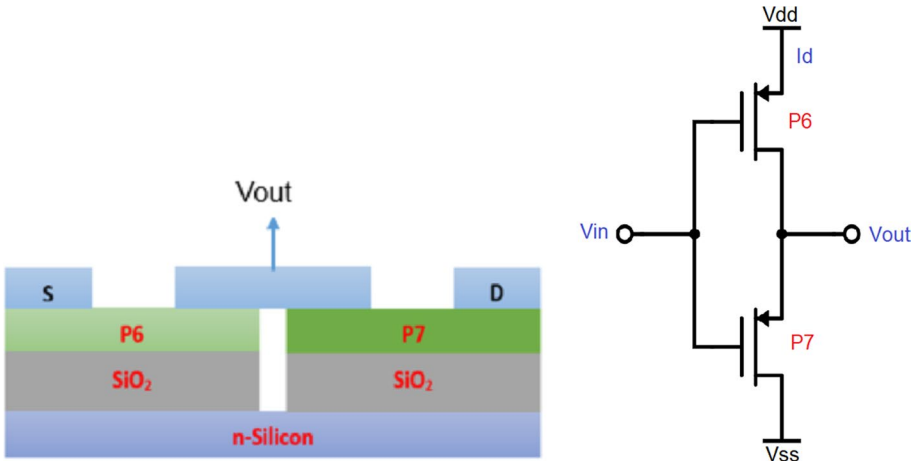

Fig. 3 Physical circuit structure and circuit schematic of P6 and P7 transistors

sum of the voltages across each OFET, and the effective gate voltages relative to source and drain voltages depended on the individual source-drain voltage drops. When the OFETs are operating in the linear regime, the circuit operates as a voltage divider circuit. Figure 4 presents the voltage transfer curve (VTC) of the series circuit. From Fig. 4, the circuit voltage output curve shows that the channel resistance of the P6 OFET in the on state is much lower than that of the P7

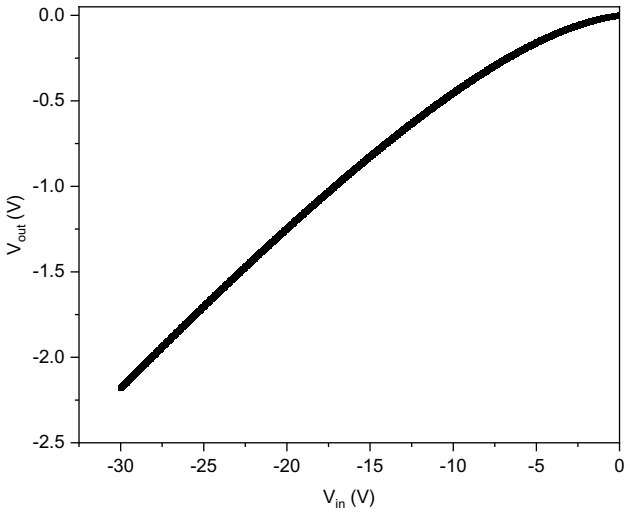

Fig. 4 Series circuit voltage transfer curve for $V_{DD}=0$, $V_{SS}=-30$ V

OFET. At −30 V gate voltage and drain voltage, the voltage drop across the P6 OFET is −2.2 V and the voltage across the P7 OFET is −27.8 V.

4 Analyte sensitivity simulation

4.1 Device sensitivity simulation

The gas sensitivity characterization of the transistors is performed in the laboratory by exposing the transistors to different concentrations of NO_2 in air [9]. Then drain current verses gate voltage measurements are taken and the results for various concentrations are compared. The corresponding simulation is done by matching current–voltage data with experiment using the doping density as a matching parameter. The variation of doping density in turn varies the charge mobility in the semiconductor. The mobility is extracted when the simulation displays best match with experiment. In both simulation and experiment, the change in drain current of the devices was used as the sensitivity (responsivity) comparison parameter for different gas concentrations. The sensitivity is calculated using the formula $(I_{d,NO2}-I_{d,air})/I_{d,air} * 100\%$, [9] where $I_{d,air}$ and $I_{d,NO2}$ are the drain currents before and after exposure to NO_2, respectively. We first investigated the NO_2 responses of P6 and P7 OFETs individually. The change in drain current for each NO_2 concentration is shown in Table 2. The data presented in the table are an average of measurements taken for 6 identical devices. The transfer curve for a typical device (for both p6 and p7) is given in Fig. 5. Measurements and simulations are performed at the drain voltage of −100 V. Figure 5a is the transfer curve for the P6 transistor and Fig. 5b is for the P7 transistor at different NO_2 concentrations. For each exposure a fresh transistor is used to measure the response of the exposure. However, all transistors are the same batch which are fabricated with the same condition at the same time. The change in drain current is the same by definition for both experiment and simulation. This is because the goal of the simulation in this particular procedure is to determine the increase in doping concentration (relative to that of pristine or unexposed OFETs) that resulted in the same changes in experimental drain current for each associated NO_2 concentration.

Table 2 Summary of OFET sensitivity for various NO_2 concentrations

NO_2 exposure (experiment)	Change in Id (%) (Expt./Sim.)		Doping (cm^{-3})	
	*P*6	*P*7	*P*6	*P*7
1 ppm	157 ± 12	10 ± 9	1.88×10^{16}	2.07×10^{14}
5 ppm	258 ± 15	53 ± 18	2.52×10^{16}	2.88×10^{14}
10 ppm	571 ± 11	99 ± 25	4.73×10^{16}	3.76×10^{14}
20 ppm	613 ± 22	192 ± 12	5.04×10^{16}	5.64×10^{14}

As shown in the table, the sensitivity of the OFET with P6 is much higher than that of the OFET with P7. At 1 ppm NO_2 concentration the sensitivity of P6 is about 15 times the sensitivity of P7. As indicated by cyclic voltammetry, the oxidation potential of P6 is less positive than that of P7. Since NO_2 responses are governed by backbone dopability, their responses would be expected to be different. Morphological factors could also contribute response differences [9]. The percentage change in doping used in simulation and the corresponding mobility extracted from simulation are also determined. Figure 6 shows the gas analyte sensitivity of P6 and P7 OFETs in terms of change in doping and mobility. Figure 6a, b are percentage changes in doping and mobility, respectively, for the P6 OFET. Similarly, Fig. 6c, d are percentage changes in doping and mobility, respectively, for the P7 OFET.

4.2 Circuit sensitivity simulation

Circuits characterized in Sect. 3.2 are simulated and tested for analyte sensitivity. The doping dependent mobility model is implemented by applying the changes in doping we observed for single transistors in Sect. 3.1. For the circuit analyte sensitivity simulation, single transistor material and model parameters presented in Table 1 are used. The single transistor doping changes that allowed for the best correspondence with the experimental observations shown in Table 2 are employed. The circuit sensitivity simulation is done for three cases: case 1 assumes only the P6 OFET is exposed to NO_2 gas; case 2 assumes only P7 is exposed to NO_2; and case 3 assumes both P6 and P7

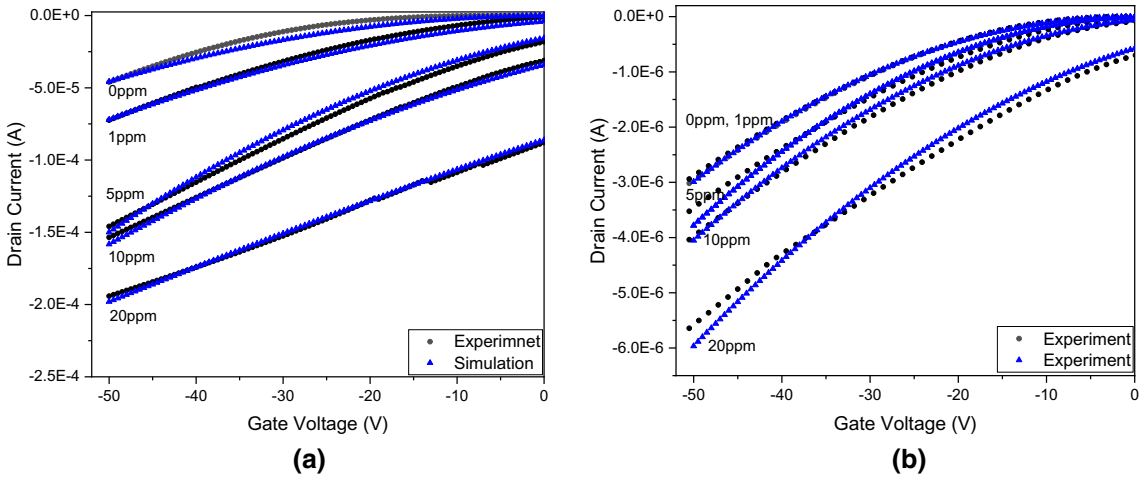

Fig. 5 **a** P6 transistor transfer characteristic for different NO_2 concentration; **b** P7 transistor transfer characteristic for different NO_2 concentration

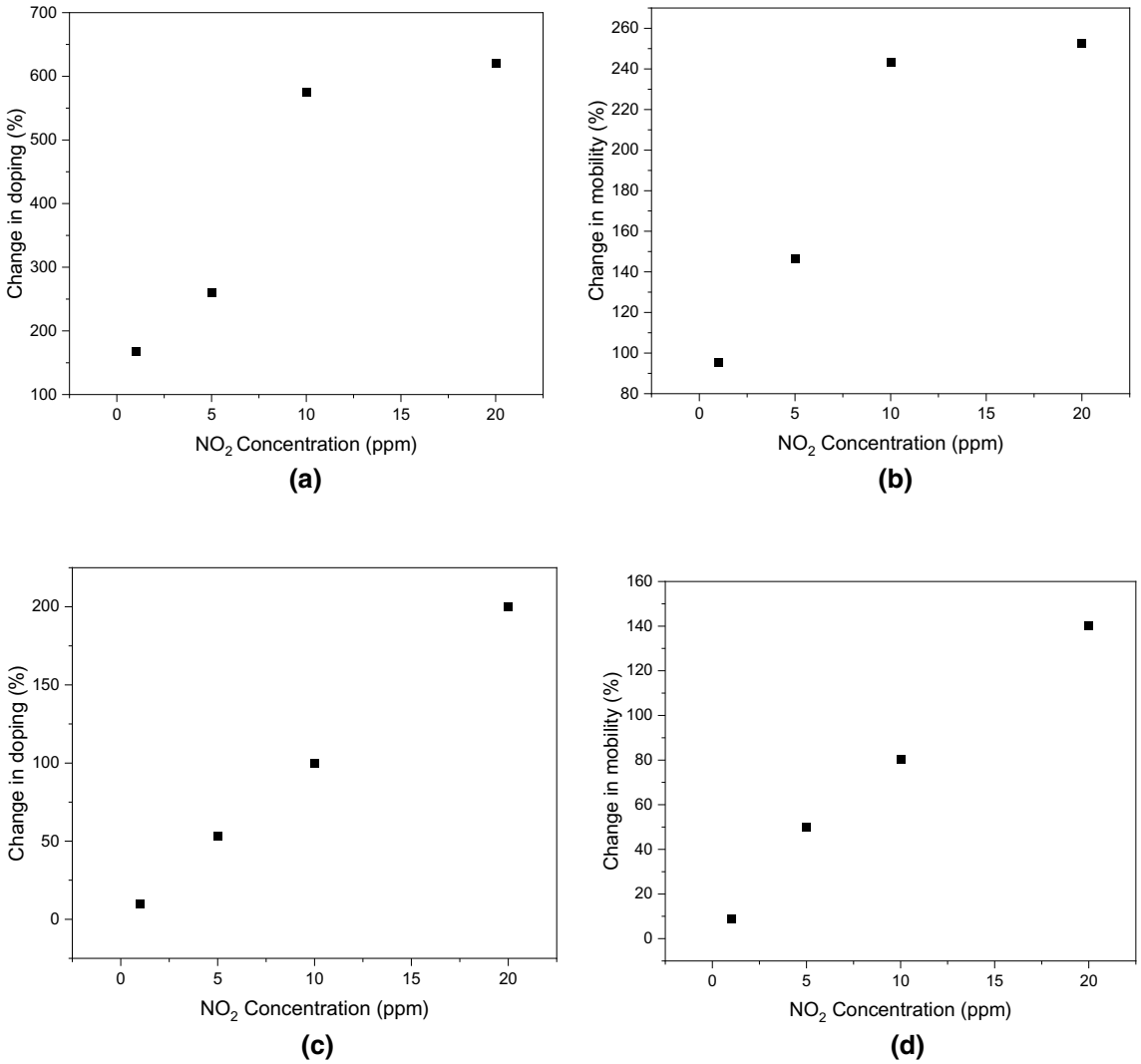

Fig. 6 Single transistor analyte sensitivity simulation, **a**, **b** P6 OFET; **c**, **d** P7 OFET

are exposed to NO_2. The simulations are performed under V_{SS} grounded in Fig. 3. Its purpose is to determine the effects of individual transistors on the overall circuit analyte sensitivity. Figure 7 presents the simulation results of the three cases. Comparing Fig. 7a–c, the sensitivity of the circuit is dominated by the sensitivity of P6 transistor. At 20 ppm NO_2 exposure, when only P6 is exposed to the gas, the circuit voltage sensitivity is 26%. However, when only P7 is exposed, the circuit sensitivity is only 4.2%. When both transistors are exposed, the circuit sensitivity follows the trends of P6 sensitivity and it is 22.4%. However, as will be seen in the next section, the value of the P7 OFET is its role in diminishing the circuit response to humidity relative to the circuit response to NO_2.

5 Humidity sensitivity simulation

5.1 Device humidity simulation

To study the stability of the OFETs against environmental effects, current–voltage measurements and simulations are performed for various humidity level exposures. Figure 8a, c (transfer curves taken at − 80 V drain voltage) present measured and simulated single transistor humidity sensitivity of P6 and P7 OFETs, respectively. The P6 OFET was exposed to a humidity ramp from 15 to 75% and displayed a current drift of 17%. The P7 OFET displayed a current drift of 31% when exposed to a humidity ramp from 25 to 63%, a comparable order of magnitude. The humidity sensitivities of the transistors are modeled by a uniform trap density with a trap energy level of 0.4 eV. In organic semiconductors, humidity

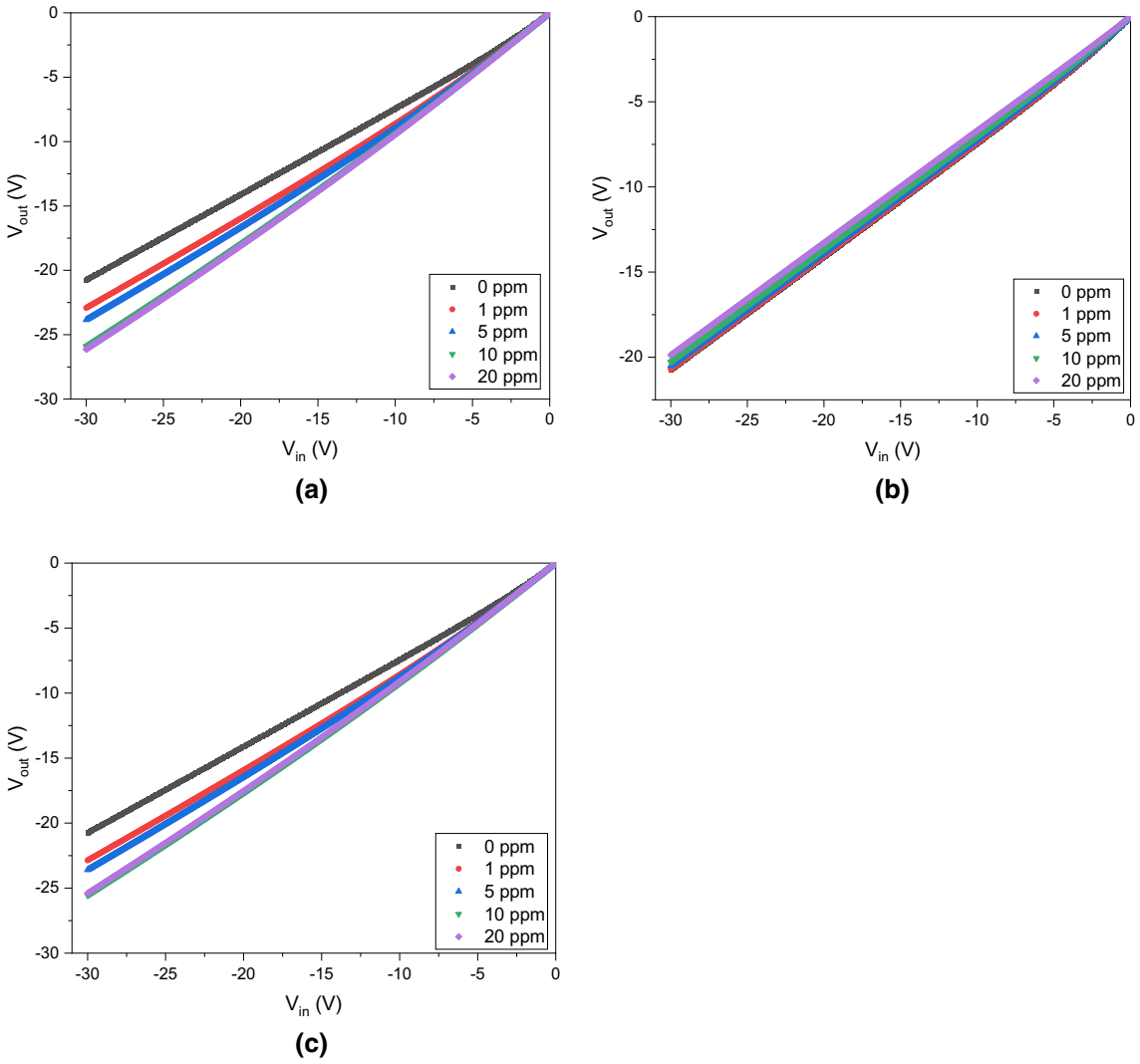

Fig. 7 Series circuit analyte sensitivity simulation **a** only P6 exposed, **b** only P7 exposed, and **c** both P6 and P7 exposed

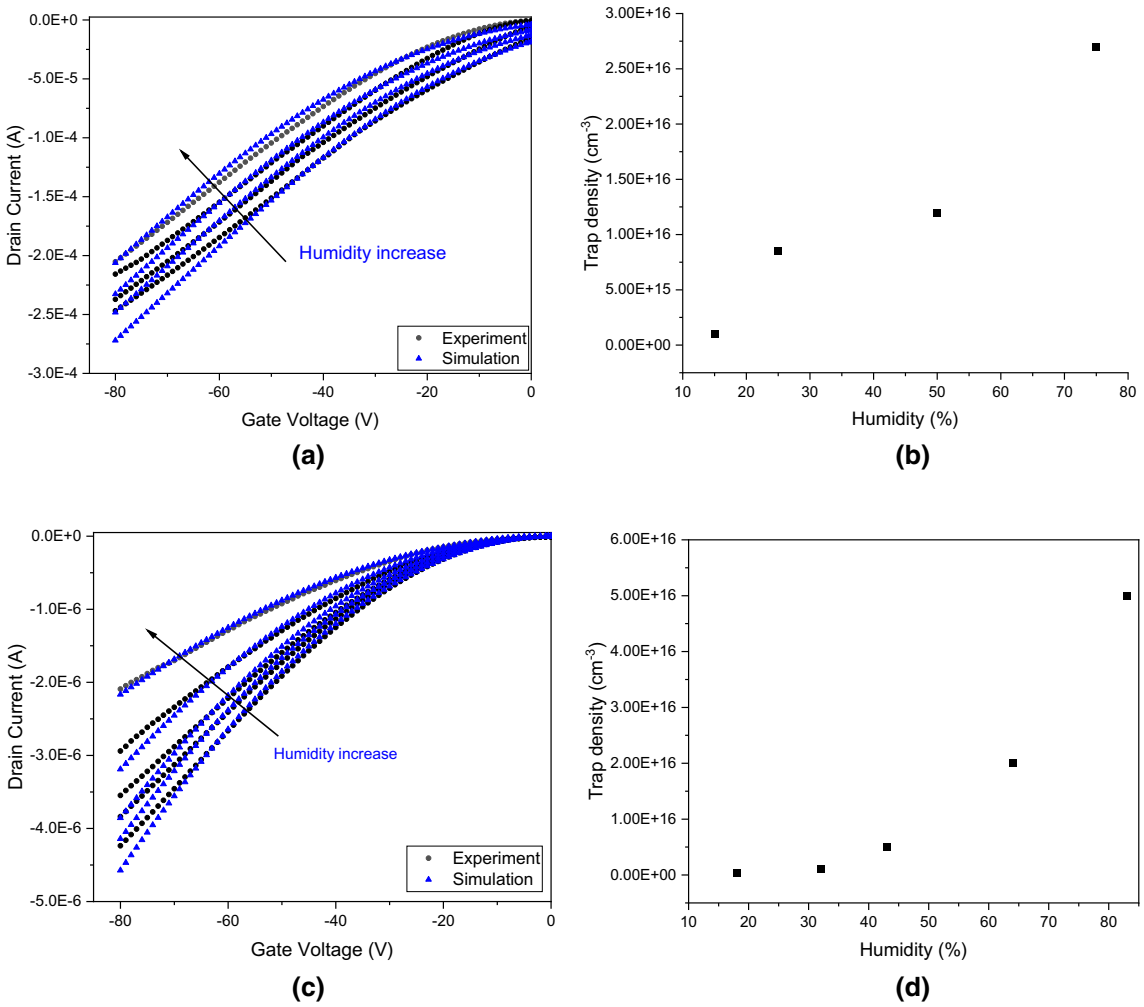

Fig. 8 Device humidity sensitivity simulation **a**, **b** P6 OFET, **c**, **d** P7 OFET

induced traps have energies in the range of 0.3–0.5 eV [51, 52]. The trap density dependence of the humidity ramp is shown in Fig. 8b, d for P6 and P7 transistors, respectively.

5.2 Circuit analyte sensitivity under humidity exposure

The main goal of this work is to study the analyte (NO_2) sensitivity performance of the series circuit under humidity exposure. The circuit configuration as shown in Fig. 3 was exposed to 15% humidity and tested for NO_2 exposure ranging from 1 to 20 ppm. The simulation is done for two cases. For case 1, the circuit is constructed from P6 and P7 OFETs having the same dimension, and we call it an asymmetric circuit. For case 2, the circuit is constructed from P6 and P7 OFETs that are designed to have matching channel resistance, which we call a symmetric circuit. The channel resistance is modeled by the linear resistance model given by Eq. (9) [53].

$$R_{\text{ch}} = \frac{1}{\mu C_{\text{ox}}\left(\frac{W}{L}\right)\left(V_{\text{DD}} - |V_{\text{TP}}|\right)} \tag{9}$$

where μ is the mobility, C_{ox} is the oxide capacitance per unit area, W is channel width, L is channel length, V_{DD} is the drain voltage, and V_{TP} is the threshold voltage.

Using the mobility and threshold voltage values given in Table 1, we matched the channel resistances of the P6 and P7 transistors (i.e., $R_{\text{chP6}} = R_{\text{chP7}}$). Based on this numerical design, the width of P7 transistor is larger than that of P6 transistor by a factor of 28. The two transistors have the same channel length and oxide capacitance per unit area. The voltage transfer curve (VTC) of the circuit in both symmetrical and asymmetrical cases is show in Fig. 9. The VTC for the symmetrical design shows approximately an equal voltage drop across the two transistors while the asymmetrical design shows a significant voltage drop across the P7 transistor.

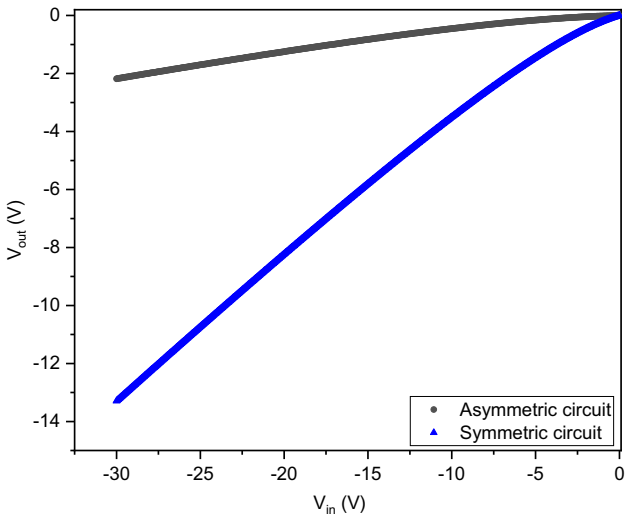

Fig. 9 Circuit voltage transfer curve (VTC) for asymmetric circuit (black circle) and symmetric circuit (blue triangle) (Color figure online)

Figure 10a presents experimental and simulation results for various NO_2 levels. In the figure, the experimental (black circles) and simulation 1 (red triangles) plots show results for the asymmetric circuit. It is observed that at 15% humidity level, the circuit maintains a robust response to NO_2. Since the two polymers have similar drifts in humidity but significantly different response to NO_2, the voltage divider circuit configuration displays a minimal humidity effect on its analyte response. The 15% humidity level of P6 and P7 transistors is simulated with 1.15×10^{15} cm^{-3} and 3.45×10^{14} cm^{-3} trap densities, respectively.

In Fig. 10a, simulation 2 (blue squares) presents the simulation prediction of NO_2 sensitivity of the circuit based on output-matched P6 and P7 transistors (symmetric circuit). For this symmetrical circuit simulation, first, we designed the circuit at 15% humidity level to have a symmetrical voltage transfer curve by adjusting the dimension of the P7 transistor. Then, we tested the humidity sensitivity of the symmetric circuit by increasing the trap density. To predict the response of the circuit for an additional 15% relative humidity level, the trap density is increased to 1.3×10^{15} cm^{-3} and 3.9×10^{14} cm^{-3} for P6 and P7 transistors, respectively.

The voltage transfer curve of the symmetric circuit is given by Fig. 10b. As shown by the inset in the figure, the output voltage variation is insignificant, changing only by 1.11%. This symmetric circuit is then studied for NO_2 response and the result is shown by simulation 2 in Fig. 10a, as described above. When the circuit is designed for symmetrical output, the simulation predicts significant improvement in analyte sensitivity for all concentrations of NO_2, used in this study. The response at 1 ppm shows more than double the sensitivity compared to that of the asymmetric circuit, and again, with humidity sensitivity reduced to insignificance. To the best of our knowledge, this is the first study of the technique of symmetrical circuit design methodology to suppress the effect of humidity on OFET circuits while maintaining their response to gas analyte. This strategy could be implemented for any type of organic field effect transistor circuit where a background signal is to be suppressed in favor of an analytical signal, and where the signals arise from defined electronic modulations.

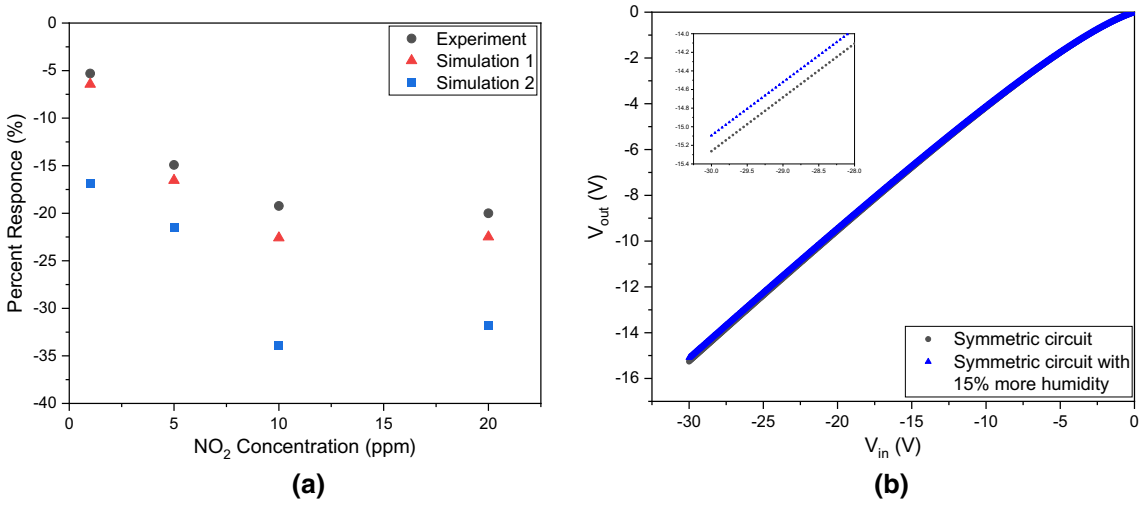

Fig. 10 **a** Circuit NO_2 sensitivity: simulation 1—asymmetric circuit, simulation 2—symmetric circuit, **b** symmetric circuit

6 Conclusion

We have investigated gas sensitivity of organic thin film transistors and circuits. P6 and P7 polymers are used for this experimental and simulation study. A two-dimensional finite element physical simulation is performed. Charge trap in the semiconductor is modeled by double peak Gaussian distribution. The doping dependent mobility model is used to model the gas sensitivity of polymers. Interface charges and traps at the interface between the semiconductor and the gate dielectric are also considered. In addition to single transistors, OFETs in series configurations are studied. Simulation results are compared with experiment and device parameters are extracted. Simulations are in good agreement with experiment. The results of this work demonstrate three important observations. The first one is modeling of analyte sensitivity of polymers using the doping dependent mobility model. The second is that the effect of humidity is modeled by traps in the semiconductor. The third observation is that the circuit from the series combination of transistors displayed a robust and enhanced sensitivity to NO_2 analyte under 15% humidity, while the response to the humidity itself was much less than it was for the individual devices. The simulation predicts significant improvement in analyte sensitivity and reduced humidity effect when the circuit is constructed from symmetric output transistors.

Appendix

OFET and circuit fabrication and testing

OFETs were fabricated using n-doped silicon wafers with a coating of 300 nm SiO_2. The substrates were cleaned and modified with HMDS self-assembled monolayers, before casting the polymers, as described in Ref. [9]. One batch of each polymer was used for the study, and experimental data are averages from several devices from each polymer, with standard deviations reported in Table 2. The individual OFETs were connected to form the circuitry via 3 M IC test fixtures. These fixtures contain clips that allow for easy manipulation and testing of the devices without destroying the evaporated electrodes on the surface. The back of the OFET was scratched to penetrate the native oxide layer of the conductive silicon wafer substrate and allow a connection point between the tip of a clip and the gate of the OFET. The gate was connected to the back of the fixture, while the source and drain electrodes were connected to the front. The OFETs were placed in a closed container made from Styrofoam to allow for the careful control of humidity and NO_2 concentration. A humidity sensor was placed to provide an accurate reading of the internal humidity. The electrodes of the 3M IC test fixtures were connected to a B1500A Keysight semiconductor device parameter analyzer via soldered wire.

Acknowledgements We gratefully acknowledge the National Science Foundation, ECCS Division, Award Number 1087293 for supporting this work.

Funding Funding source declared above in the acknowledgment section.

Availability of data and materials The datasets generated during and/or analyzed during the current study are available from the corresponding author on reasonable request.

Code availability Not applicable.

Declarations

Conflict of interest The authors have no relevant financial or non-financial interests to disclose.

References

1. Guo, X., Xu, Y., Ogier, S., Ng, T.N., Caironi, M., Perinot, A., Li, L., Zhao, J., Tang, W., Sporea, R., Nejim, A., Carrabina, J., Cain, P., Yan, F.: Current status and opportunities of organic thin-film transistor technologies. IEEE Trans. Electron Devices **64**(5), 1906–1921 (2017)
2. Matsui, H., Takeda, Y., Tokito, S.: Flexible and printed organic transistors: from materials to integrated circuits. Org. Electron. **75**, 105432–105432 (2019)
3. Dimitrakopoulos, C.D., Mascaro, D.J.: Organic thin-film transistors: a review of recent advances. IBM J. Res. Dev. **45**(1), 11–27 (2001)
4. Khan, S., Lorenzelli, L., Dahiya, R.S.: Technologies for printing sensors and electronics over large flexible substrates: a review. IEEE Sens. J. **15**(6), 3164–3185 (2015). https://doi.org/10.1109/JSEN.2014.2375203
5. Sophocleous, M., Contat-Rodrigo, L., García-Breijo, E., Georgiou, J.: Organic electrochemical transistors as an emerging platform for bio-sensing applications: a review. IEEE Sens. J. **21**(4), 3977–4006 (2021). https://doi.org/10.1109/JSEN.2020.3033283
6. Stagni, C., Guiducci, C., Benini, L., Riccò, B., Carrara, S., Samorí, B., Paulus, C., Schienle, M., Augustyniak, M., Thewes, R.: CMOS DNA sensor array with integrated A/D conversion based on label-free capacitance measurement. IEEE J. Solid-State Circuits **41**(12), 2956–2964 (2006). https://doi.org/10.1109/JSSC.2006.884867
7. Carrara, S., Ghoreishizadeh, S., Olivo, J., Taurino, I., Rossi, C.B., Cavallini, A., Beeck, M.O.D., Dehollain, C., Burleson, W., Moussy, F.G., Guiseppi-Elie, A., Micheli, D.: Fully integrated biochip platforms for advanced healthcare. Sensors **12**, 11013–11060 (2012)
8. Yaghmazadeh, O., Cicoira, F., Bernards, D.A., Yang, S.Y., Bonnassieux, Y., Malliaras, G.G.: Optimization of organic electrochemical transistors for sensor applications. J. Polym. Sci. Part B Polym. Phys. **49**, 34–39 (2011)

9. Mukhopadhyaya, T., Wagner, J., Fan, H., Katz, H.E.: Design and synthesis of air-stable p-channel-conjugated polymers for high signal-to-drift nitrogen dioxide and ammonia sensing. ACS Appl. Mater. Interfaces **12**(19), 21974–21984 (2020)
10. Tremblay, N.J., Jung, B.J., Breysse, P., Katz, H.E.: Digital-inverter amine sensing via synergistic responses by n and p organic semiconductors. Adv. Funct. Mater. **21**, 4314–4319 (2011)
11. Besar, K., Dailey, J., Zhao, X., Katz, H.E.: A flexible organic inverter made from printable materials for synergistic ammonia sensing. J. Mater. Chem. **5**, 6506–6511 (2017)
12. Li, M.-Z., Han, S.-T., Zhou, Y.: Recent advances in flexible field-effect transistors toward wearable sensors. Adv. Intell. Syst. **2**, 2000113–2000138 (2020)
13. Petritz, A., Wolfberger, A., Fian, A., Krenn, J.R., Griesser, T., Stadlober, B.: High performance p-type organic thin film transistors with an intrinsically photopatternable, ultrathin polymer dielectric layer. Org. Electron. **14**, 3070–3082 (2013)
14. Egginger, M., Irimia-Vladu, M., Schwödiauer, R., Tanda, A., Frischauf, I., Bauer, S., Sariciftci, N.S.: Mobile ionic impurities in poly(vinyl alcohol) gate dielectric: possible source of the hysteresis in organic field-effect transistors. Adv. Mater. **20**, 1018–1022 (2008)
15. Montaigne Ramil, A., Hernandez-Sosa, G., Griesser, T., Simbrunner, C., Hoefler, T., Trimmel, G., Kern, W., Shen, Q., Teichert, C., Schwabegger, G., Sitter, H., Sariciftci, N.S.: Photo-Fries-based photosensitive polymeric interlayers for patterned organic devices. Appl. Phys. A **107**, 985–993 (2012)
16. Zhang, C., Chen, P., Hu, W.: Organic field-effect transistor-based gas sensors. Chem. Soc. Rev. **44**, 2087–2107 (2015)
17. Wang, C., Dong, H., Hu, W., Liu, Y., Zhu, D.: Semiconducting π-conjugated systems in field-effect transistors: a material odyssey of organic electronics. Chem. Rev. **112**, 2208–2267 (2012)
18. Sirringhaus, H.: 25th anniversary article: organic field-effect transistors: the path beyond amorphous silicon. Adv. Mater. **26**, 1319–1335 (2014)
19. Di, C.-A., Liu, Y., Yu, G., Zhu, D.: Interface engineering: an effective approach toward high-performance organic field-effect transistors. Acc. Chem. Res. **42**, 1573–1583 (2009)
20. Wondmagegn, W., Chu, Y., Li, H., Katz, H.E., Huang, J.: Simulation of two-transistor parallel and series circuits for gas sensing validated by experimental data. J. Comput. Electron. **20**, 626–634 (2020)
21. Vladimirov, I., Kühn, M., Gebner, T., May, F., Weitz, R.T.: Energy barriers at grain boundaries dominate charge carrier transport in an electron-conductive organic semiconductor. Sci. Rep. **8**, 14868–14877 (2018)
22. Rani, V., Sharma, A., Kumar, P., Singh, B., Ghosh, S.: Charge transport mechanism in copper phthalocyanine thin films with and without traps. RSC Adv. **7**, 54911–54919 (2017)
23. Hartenstein, B., Bassler, H., Jakobs, A., Kehr, K.W.: Comparison between multiple trapping and multiple hopping transport in a random medium. Phys. Rev. B Condens. Matter Mater. Phys. **54**, 8574–8579 (1996)
24. Horowitz, G.: Organic field-effect transistors. Adv. Mater. **10**, 365–377 (1998)
25. Vissenberg, M.C.J.M., Matters, M.: Theory of the field-effect mobility in amorphous organic transistors. Phys. Rev. B Condens. Matter Mater. Phys. **57**, 12964–12967 (1998)
26. Ha, D.-G., Kim, J.-J., Baldo, M.A.: Link between hopping models and percolation scaling laws for charge transport in mixtures of small molecules. AIP Adv. **6**(045221), 1–5 (2016)
27. Guo, D., Miyadera, T., Ikeda, S., Shimada, T., Saiki, K.: Analysis of charge transport in a polycrystalline pentacene thin film transistor by temperature and gate bias dependent mobility and conductance. J. Appl. Phys. **102**, 023706 (2007)
28. Kumar, V., Jain, S., Kapoor, A., Poortmans, J., Mertens, R.: Trap density in conducting organic semiconductors determined from temperature dependence of J-V characteristics. J. Appl. Phys. **94**, 1283–1285 (2003)
29. Agrawal, R., Kumar, P., Ghosh, S., Mahapatro, A.K.: Thickness dependence of space charge limited current and injection limited current in organic molecular semiconductors. Appl. Phys. Lett. **93**, 073311 (2008)
30. Bassler, H.: Charge transport in disordered organic photoconductors a Monte Carlo simulation study. Phys. Status Solidi B **175**, 15–56 (1993)
31. Sharma, A., Yadav, S., Kumar, P., Chaudhuri, S.R., Ghosh, S.: Defect states and their energetic position and distribution in organic molecular semiconductors. Appl. Phys. Lett. **102**, 143301 (2013)
32. Hegedus, S.S., Fagen, E.A.: Midgap states in a-Si: H and a-SiGe: H p-i-n solar cells and Schottky junctions by capacitance techniques. J. Appl. Phys. **71**, 5941–5951 (1992)
33. Milani, L., Torricelli, F., Kovacs-Vajna, Z.M., Colalongo, L.: Comparison between mobility models in organic semiconductors. In: Proceedings of the International Conference on Organic Electronics (ICOE 2011), 22–24 June 2011, Rome, Italy, pp. 54–55
34. Criteria Air Pollutants | US EPA. https://www.epa.gov/criteria-air-pollutants. Accessed 18 Aug 2021
35. Dong, Q., Li, B., Downen, R.S., Tran, N., Chorvinsky, E., Pillai, D.K., Zaghloul, M.E., Li, Z.: A cloud-connected NO_2 and ozone sensor system for personalized pediatric asthma research and management. IEEE Sens. J. **20**(24), 15143–15153 (2020)
36. Novikov, S., Lebedeva, N., Satrapinski, A., Walden, J., Davydov, V., Lebedev, A.: Graphene based sensor for environmental monitoring of NO_2. Sens. Actuators B **236**, 1054–1060 (2016)
37. Afshar-Mohajer, N., Zuidema, C., Sousan, S., Hallett, L., Tatum, M., Rule, A.M., Thomas, G., Peters, T.M., Koehle, K.: Evaluation of low-cost electro-chemical sensors for environmental monitoring of ozone, nitrogen dioxide, and carbon monoxide. Occup. Environ. Hyg. **15**(2), 87–98 (2018)
38. ATLAS User's Manual. Silvaco International, Santa Clara (2007)
39. Robertson, J.: High dielectric constant oxides. Eur. Phys. J. Appl. Phys. **28**, 265–291 (2004)
40. Giustino, F., Umari, P., Pasquarello, A.: Dielectric effect of a thin SiO2 interlayer at the interface between silicon and high-k oxides. Microelectron. Eng. **72**, 299–303 (2004)
41. Sprague, J.L., Minahan, J.A., Wied, O.J.: Physical and dielectric properties of the metal-silicon dioxide-silicon system. J. Electrochem. Soc. **109**, 94–98 (1962)
42. Moore, G.: Progress in digital integrated electronics. In: IEEE Electron Devices Meeting 11–13 (1975)
43. Rozenberg, M., Inoue, I., Sanchez, M.: Nonvolatile memory with multilevel switching: a basic model. Phys. Rev. Lett. **92**, 17 (2004)
44. Knapp, E., Häusermann, R., Schwarzenbach, H.U., Ruhstaller, B.: Numerical simulation of charge transport in disordered organic semiconductor devices. J. Appl. Phys. **108**, 054504 (2010)
45. Arkhipov, V.I., Heremans, P., Emelianova, E.V., Adriaenssens, G.J., Bässler, H.: Charge carrier mobility in doped semiconducting polymers. Appl. Phys. Lett. **82**, 3245–3247 (2003)
46. Higgins, A., Mohapatra, S.K., Barlow, S., Marder, S.R., Kahn, A.: Dopant controlled trap-filling and conductivity enhancement in an electron-transport polymer. Appl. Phys. Lett. **106**, 163301 (2015)
47. Olthof, S., Mehraeen, S., Mohapatra, S.K., Barlow, S., Coropceanu, V., Brédas, J.-L., Marder, S.R., Kahn, A.: Ultralow doping in organic semiconductors: evidence of trap filling. Phys. Rev. Lett. (2012). https://doi.org/10.1103/PhysRevLett.109.176601

48. Shirinskaya, A., Horowitz, G., Rivnay, J., Malliaras, G.G., Bonnassieux, Y.: Numerical modeling of an organic electrochemical transistor. Biosensors **103**, 1–14 (2018)
49. Friedlein, J.T., Shaheen, S.E., Malliaras, G.G., McLeod, R.R.: Optical measurements revealing nonuniform hole mobility in organic electrochemical transistors. Adv. Electron. Mater. **1**, 1500189–1500197 (2015)
50. Arkhipov, V.I., Emelianova, E.V., Adriaenssens, G.J.: Effective transport energy versus the energy of most probable jumps in disordered hopping systems. Phys. Rev. B **64**, 1–6 (2001)
51. Zuo, G., Linares, M., Upreti, T., Kemerink, M.: General rule for the energy of water-induced traps in organic semiconductors. Nat. Mater. **18**, 588–593 (2019)
52. Steiger, J., Karg, S., Schmechel, R., Seggern, H.V.: Aging induced traps in organic semiconductors. Synth. Met. **122**(1), 49–52 (2001)
53. John, U.P.: Electrical Characteristics of MOSFETs. Introduction to VLSI Circuits and Systems, Ch 6, pp. 191–235. Wiley, New York (2002)